

Exploring and understanding 2D microwave near-fields using a single ion

M. Wahnschaffe,^{1,2,3} H. Hahn,^{1,2} G. Zarantonello,^{1,2} T. Dubielzig,²
S. Grondkowski,² A. Bautista-Salvador,^{1,2,3} M. Kohlen,^{1,2,3} and C. Ospelkaus^{1,2,3}

¹*Physikalisch-Technische Bundesanstalt, Bundesallee 100, 38116 Braunschweig, Germany*

²*Institute of Quantum Optics, Leibniz Universität Hannover, Welfengarten 1, 30167 Hannover, Germany*

³*Laboratory for Nano- and Quantum Engineering,*

Leibniz Universität Hannover, Schneiderberg 39, 30167 Hannover, Germany

We develop an intuitive model of 2D microwave near-fields in the unusual regime of centimeter waves localized to tens of microns. Close to an intensity minimum, a simple effective description emerges with five parameters which characterize the strength and spatial orientation of the zero and first order terms of the near-field, as well as the field polarization. Such a field configuration is realized in a microfabricated planar structure with an integrated microwave conductor operating near 1 GHz. We use a single $^9\text{Be}^+$ ion as a high-resolution quantum sensor to measure the field distribution through energy shifts in its hyperfine structure. We find agreement with simulations at the sub-micron and few-degree level. Our findings give a clear and general picture of the basic properties of oscillatory 2D near-fields with applications in quantum information processing, neutral atom trapping and manipulation, chip-scale atomic clocks, and integrated microwave circuits.

PACS numbers: 03.67.Bg, 03.67.Lx, 37.10.Rs, 37.10.Ty, 37.90.+j

Static or oscillatory electromagnetic fields have important applications in atomic and molecular physics for atom trapping and manipulation. Neutral atoms can be trapped in static magnetic fields in different types of magnetic traps [1]. Atomic ions can be trapped either in superpositions of static and oscillatory electric fields (Paul trap) or in superimposed static electromagnetic fields (Penning trap) [2]. Atom and molecule decelerators rely on the distortion of atomic energy levels by spatially inhomogeneous fields [3]. Common to all of these field configurations is that their basic properties can be well described in terms of static solutions to the field equations and that the behavior of the field near its intensity minimum is often critical to the application. Prominent examples include Majorana losses in neutral atom magnetic traps [1] and micromotion in Paul traps [4].

Recently, motivated by advances in microfabricated atom traps, interest has grown in microwave near-fields which originate from microfabricated structures. Dimensions are typically small compared to the wavelength, but for the relatively high frequencies involved, eddy currents and phase effects become important, and the resulting field patterns are much richer than in the quasistatic case. Examples include rf potentials for neutral atoms [5] with applications in atom interferometry, quantum gates [6, 7] and chip-scale atomic clocks [8] as well as microwave near-fields for trapped-ion quantum logic [9–11]. Also, neutral atomic clouds [12] and single ions [13] have been used to characterise near-fields at sub-mm length scales or measure magnetic field gradients [14]. The behavior of these high-frequency oscillatory fields may also become relevant for coupling atomic and molecular quantum systems to microwave circuits in the quantum regime [15, 16]. Of particular importance in this context are 2D field configurations which can be

realized e. g. in integrated waveguides. Notwithstanding the strong experimental interest, there is a lack of intuitive understanding and the wide-spread notion that numerical simulation of microwave near-fields originating from such structures is difficult and potentially error prone near a field minimum.

Here we develop a simple picture of 2D microwave fields around a local minimum of the field intensity and confirm this model through numerical simulations and experimental measurements involving a microfabricated ion trap with an integrated microwave conductor. We assume that the dimensions are small compared to the wavelength, so that $\text{div} \vec{B} = 0$ and $\text{rot} \vec{B} = 0$ (near-field condition). Expansion of a 2D field up to first order would in principle result in a total of 6 complex or 12 real-valued expansion coefficients. However, taking into account the near-field condition, we can write the magnetic field in terms of eight parameters: $B_{r,i}$ and $\alpha_{r,i}$, characterizing the real and imaginary components of the complex field at the origin and their spatial orientations, and $B'_{r,i}$ and $\beta_{r,i}$, which describe the real and imaginary components of the complex field gradient and their spatial orientations:

$$(1) \quad \vec{B} = \text{Re} \left\{ e^{i\omega t} \left[(B_r \vec{e}_{\alpha_r} + i B_i \vec{e}_{\alpha_i}) + (B'_r Q_{\beta_r} + i B'_i Q_{\beta_i}) \vec{r} + \dots \right] \right\},$$

$$\vec{e}_{\alpha} \equiv \begin{pmatrix} \cos \alpha \\ \sin \alpha \end{pmatrix} \quad \text{and} \quad Q_{\beta} \equiv \begin{pmatrix} \cos \beta & \sin \beta \\ \sin \beta & -\cos \beta \end{pmatrix},$$

where Q_{β} is a traceless and symmetric “quadrupole matrix” to ensure the near-field condition. By multiplying Eq. (1) with a suitably chosen complex phase factor, it is possible to maximize the strength of the real part of the gradient. The same choice of phase factor also leads to

$\beta_i = \beta_r - \pi/2$. We now write $(B_r, B_i) = B(\cos \varphi, \sin \varphi)$ and $(B'_r, B'_i) \equiv B'(\cos \psi, \sin \psi)$. A suitable choice for the domain of the parameters is $B, B' \in \mathbb{R}$, $\alpha_r, \beta_r, \psi \in [0, \pi[$, $\alpha_i, \beta_i, \varphi \in [-\pi/2, \pi/2[$. Further imposing the condition that $|\vec{B}|$ has a minimum at the origin leads to $\alpha_i - \alpha_r + \pi/2 = n \cdot \pi$ with $n \in \mathbb{Z}$. For our choice of parameters, the left-hand side must be in $]-\pi, \pi[$, and thus $n = 0$ and also $\alpha_i = \alpha_r - \pi/2$. Also from $|\vec{B}|$ minimal at the origin, we find $\varphi = \psi - \pi/2$. With $\alpha \equiv \alpha_r$ and $\beta \equiv \beta_r$, the field is finally given by

$$(2) \quad \vec{B} = \text{Re} \left\{ e^{i\omega t} \left[B (\vec{e}_\alpha \sin \psi - i \vec{e}_{\alpha-\pi/2} \cos \psi) + B' (Q_\beta \cos \psi + i Q_{\beta-\pi/2} \sin \psi) \vec{r} + \dots \right] \right\}$$

with just five free parameters – the strengths B and B' of the offset field and of the gradient, respectively, one angle α and β each for their spatial orientation, and an angle ψ characterizing the relative strength of the real and imaginary part of the gradient (and thus the polarization). The reduction from eight to five parameters compared to Eq. (1) is due to the assumption of a specific phase and of a minimum of $|\vec{B}|$ at the origin.

To give a specific example, consider the surface-electrode trap structure shown in Fig. 1a), a design evolved from [17]. A microwave near-field at 1.093 GHz originates from a current coupled into the meander-shaped conductor indicated by MW and terminated to ground (GND). Fig. 1b) shows the simulated surface current distribution $|\vec{J}_s|$ and the resulting distribution of $|\vec{B}|$ with a minimum at the position indicated by (*). We simulate the structure, including parts of the surrounding connector board, using Ansys HFSS. We determine the parameters of the 2D quadrupole field of Eq. (2) by fitting a 10th order polynomial to the complex \vec{B} fields in the xz plane within a $8 \mu\text{m}$ square area around the minimum and retaining only the zero and first order terms. The simulations show that all y field components are much smaller than x and z components and thus validate the assumption of a 2D field configuration. The resulting parameters of Eq. (2) are shown in Table I. Note that B, B' depend on the input current, and hence only B/B' is given. Because ψ is small, the real part of the quadrupole is rather strong, which means that the polarization is mostly linear. The dominant contribution to the gradient stems from the three conductor segments forming the meander MW, while the offset field, which is $\pi/2$ out of phase with the gradient, results from inductive coupling to neighboring metal patches and the associated eddy currents, as well as from phase delays along the meander [17].

The trap is composed of electroplated gold electrodes of $11 \mu\text{m}$ Au with $5 \mu\text{m}$ wide gaps between the electrodes on top of an AlN substrate [18]. It is located in a room temperature vacuum enclosure evacuated to

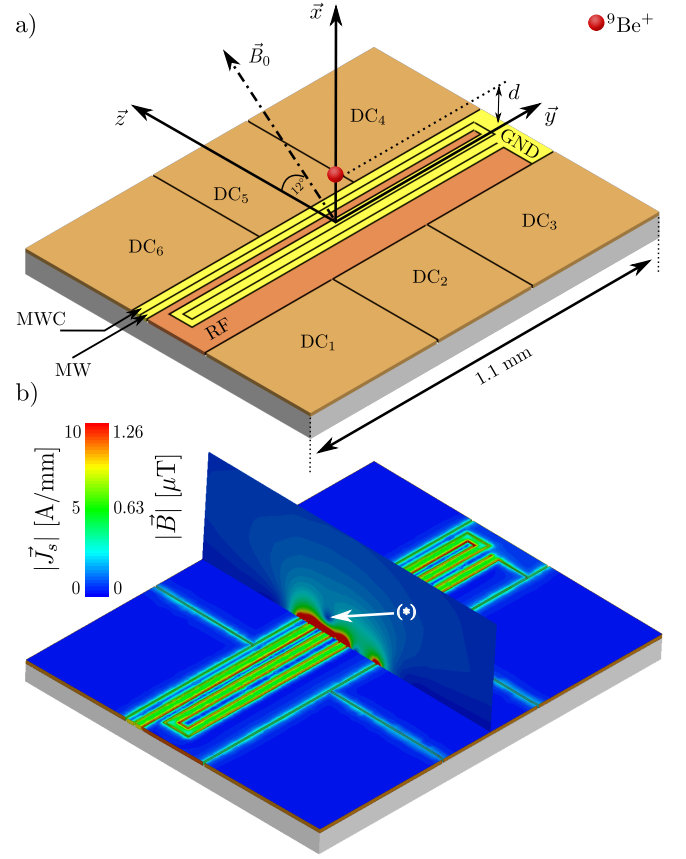


FIG. 1: a) Surface-electrode trap with embedded microwave conductor MW, leading to the surface-current distribution $|\vec{J}_s|$ and magnetic near-field $|\vec{B}|$ of b). We probe the near-field using a single $^9\text{Be}^+$ ion trapped $45 \mu\text{m}$ above the surface by applying rf and DC voltages to the electrodes RF and DC_{1–6}. Microwave signals applied to MWC are used to transfer the ion within the hyperfine manifold of Fig. 2. For clarity, the height of the ion above the surface has been exaggerated in a).

$\approx 1 \cdot 10^{-11}$ mbar. To characterize the near-field generated by the conductor MW experimentally, we employ a single $^9\text{Be}^+$ ion trapped above the structure. An rf voltage of 88 MHz frequency and 50 V amplitude is applied to the electrode labelled as RF. The resulting pseudopotential has a radial minimum at $(x, z) = (45.7, 2.9) \mu\text{m}$. Static potentials, applied to the electrodes labelled as DC_{1–6}, create a potential minimum at $y = 0$ in the axial (y) direction. By varying the applied static potentials, the ion's position can be adjusted in the radial plane. The trap depth is 39 meV, the axial trap frequency $\omega_{\text{ax}} \simeq 2\pi \cdot 1$ MHz, and the radial pseudopotential trapping frequency $\omega_{\text{rad}} \simeq 2\pi \cdot 11$ MHz. We load single ions by hitting a solid ^9Be target with single pulses of a nanosecond pulsed laser at 1064 nm and by subsequent resonant two-photon ionization at 235 nm [19, 20] from the resulting ablation plume. Ions are laser cooled and detected using light resonant

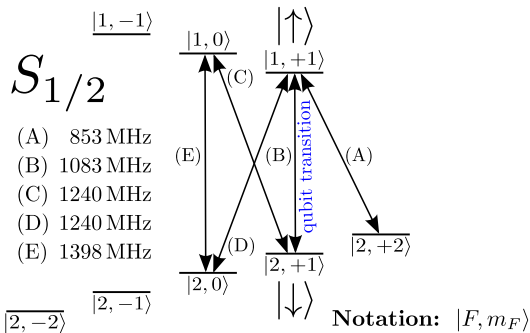


FIG. 2: Hyperfine structure of the $^9\text{Be}^+$ ground state at 22.3 mT, where transition (B) is a first-order magnetic-field independent qubit transition.

with the cycling transition $|S_{1/2}, F=2, m_F=2\rangle \rightarrow |P_{3/2}, m_J=+3/2, m_I=+3/2\rangle$ at 313 nm. We apply a static bias field \vec{B}_0 in the yz plane and at an angle of 12° with respect to the z axis to lift the degeneracy of the hyperfine levels. At the experimental value of $B_0 = 22.3$ mT, the state combination $|F=2, m_F=1\rangle$ and $|F=1, m_F=1\rangle$ forms a first order magnetic-field independent qubit [21] which can be exploited for long coherence times. Laser cooling prepares the ion in $|F=2, m_F=2\rangle$. Through a series of microwave π pulses on the conductor MWC (cf. Fig.1a)), resonant with suitable hyperfine transitions, we can prepare an arbitrary target state within the $S_{1/2}$ hyperfine manifold of Fig. 2, and determine the population of an arbitrary state by transferring it back to $|F=2, m_F=2\rangle$ and subsequently detecting fluorescence photons scattered on the cycling transition.

We determine properties of the microwave near-field through AC Zeeman energy shifts which it induces on suitable transitions in the atomic hyperfine structure, analogous to AC Stark shifts employed e. g. in optical dipole traps for neutral atoms. By measuring the influence of the near-field on different transitions within the structure of Fig. 2 with a different dependence on the field components, we are able to reconstruct the parameters of Eq. (2). We apply a signal to electrode MW blue-detuned by 10 MHz from transition (B) (see Fig. 2), and measure the influence of this signal on the frequency of (E) and (B) because it allows us to obtain complementary information on (E) B' , B and the position of the minimum vs. (B) α, β, ψ . To appreciate the effect of the near-field on the atomic energy levels, consider a frame where the z direction corresponds to \vec{B}_0 . We need to distinguish between π (parallel to \vec{B}_0) and σ (right or left circular) components of the oscillating magnetic field. For transition (E), the MW field will be red detuned from all relevant transitions allowed by selection rules, so that the net shift of (E) will always be a blue shift. For transition (B), however, the MW field is blue detuned from (B) and the π component will thus red shift

Parameter	Simulation	Experimental data
B/B'	$8.5 \mu\text{m}$	$8.7(1.0) \mu\text{m}$
ψ	6.4°	$4.3(1.2)^\circ$
α	24.3°	$31.1(3)^\circ$
β	99.9°	$109.1(11.5)^\circ$
x_0	$45.5 \mu\text{m}$	$45.3(1) \mu\text{m}$
z_0	$-0.8 \mu\text{m}$	$-0.8(2) \mu\text{m}$

TABLE I: Parameters of the microwave near-fields according to Eq. (2), determined from simulations and from experimental measurements using a single ion (Fig. 3).

the frequency of (B). In our experiment, the fields perpendicular to \vec{B}_0 are mostly linearly polarized (ψ small), which implies about equal contributions of σ^+ and σ^- . These will lead to a red shift of (B) as a result of the blue-detuned off-resonant coupling to (A). There will also be a stronger blue shift of (B) as a result of the red-detuned off-resonant coupling to (C) and (D). Thus, altogether, for (B), there will be a strong red shift as a result of the π field and a weaker blue shift as a result of the σ components.

While in principle these shifts could be measured using Rabi spectroscopy, we employ the Ramsey method described in [13] because it lends itself to easy automation. It does, however, not directly reveal the sign of the Zeeman shifts. This is not an issue for the measurements presented here, and in the following, we will always show positive signs of the net shifts. The first column of Fig. 3 shows AC Zeeman shifts of transitions (B) (top) and (E) (bottom) as a function of x and z , measured using a single ion. For transition (E), the AC Zeeman shift should exhibit a minimum close to the minimum of $|\vec{B}|$. It is also evident from Fig. 3a) that the data for transition (B) exhibits a more complex structure, which is a result of the interplay between red and blue shifts from the π and σ components.

Agreement with the numerical simulations of Table I can be tested quantitatively using a least squares fit of the AC Zeeman shifts resulting from Eq. (2) to the experimental data. The calculated AC Zeeman shifts which result from the fitted model are plotted in the right column of Fig. 3. As fit parameters, in addition to the ones of Eq. (2), we use x_0 and z_0 , the position of the minimum of $|\vec{B}|$. Data for transition (E) was taken at a power level that was nominally 6 dB higher than for (B) in order to reach higher frequency shifts. Thus, we also fitted the experimental power ratio between Fig. 3c) and a), yielding 6.47(15) dB. Experimental and fitted data have been scaled to the power level of Fig. 3a). As can be seen from Table I, the agreement between simulations and experiment is at the sub-micron and few-degree level. This is remarkable given the complicated interplay of primary and induced currents in this microfabricated structure

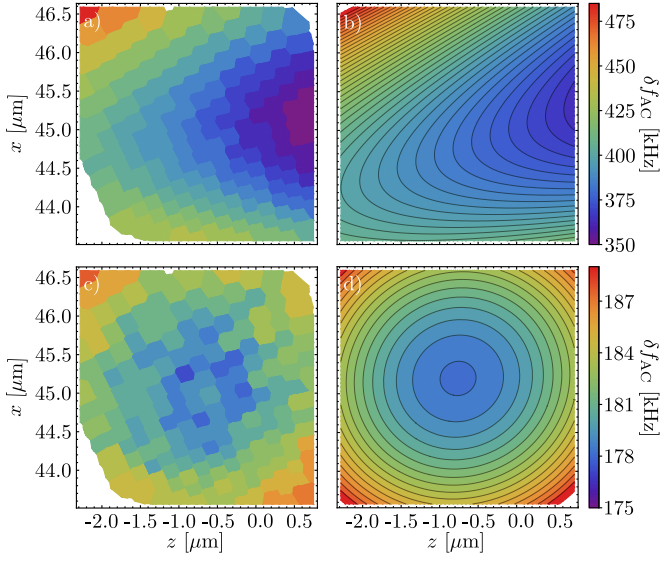


FIG. 3: AC Zeeman shifts δf_{AC} induced by 2D near-fields on a single ion. The two rows show data for transition (B) and (E) of Fig. 2, respectively. The first column shows AC Zeeman shifts measured using a single ion, and the second column shows result of a fit of Eq. (2) to the experimental data. White indicates areas in the radial plane where we cannot stably trap ions.

where the properties of the field around the minimum essentially result from the subtraction of rather large contributions from individual conductors [9, 17]. We have validated the fitting procedure by extracting magnetic field data from our numerical simulations on a grid similar to that of the experimental data, computing the AC Zeeman shifts and fitting the model to the shifts. We find that in this case, the fitting procedure perfectly reproduces the quadrupole parameters extracted directly from the numerical data.

An issue which may cause the fitted parameters to deviate slightly from the simulations is the accuracy of the assumed spatial position of the ion as a function of trap voltages applied. The position was extracted from electrostatic simulations and the pseudopotential approximation. Also, in our simulations, we found that spurious couplings to the electrode MWC had a rather strong influence on B/B' . There is a $\approx 10\%$ coupling from the MW to the MWC conductor. The value of B/B' therefore depends on the assumed termination on the MWC input. For our simulations, we assumed that about 5% of the total power coupling from the MW to the MWC conductor were reflected back into the structure. This is not an unreasonably high value, given a number of impedance changes which occur between the structure of Fig. 1 and the amplifier connected to MWC.

In summary, we have developed an intuitive model of 2D microwave quadrupole fields around a local minimum of $|\vec{B}|$, performed accurate numerical simulations of a 2D

near-field structure, and confirmed their accuracy at the sub-micron and few-degree level using a single ion as a local field probe. This description is applicable not only to microwave, but also to lower frequency rf fields. Our findings may be applicable to integrated microwave circuits and hybrid quantum approaches coupling ions to other microwave or rf quantum devices [15, 16]. Our results will inform the design of new structures for microwave quantum logic applications [9–11, 22–24] of trapped ions. Here, a lower value of B/B' would be desirable to suppress the influence of off-resonant carrier excitations in entangling quantum logic gates [9]. Towards this end, the MWC electrode should be removed or moved much further away from the trap center. In general, we find that boundary conditions and the induced currents in the entire trap structure have a profound influence. Ideally, future designs would be based on a multi-layer structure [25–27], so that signals could be delivered in layers underneath the structure via embedded waveguides and only brought to the surface close to the ion [28]. This would decouple the design of near-field structures from other trap “modules” on a scalable trap array [29] for quantum simulation [30, 31] or quantum logic applications [32, 33].

We are grateful for useful discussions with P. O. Schmidt, the NIST ion storage group, the Oxford ion trapping group and J. Schöbel. We acknowledge contributions by C. Vollmer in an early stage of the experiment, support by the PTB clean room facility team, packaging support by F. Schmidt-Kaler’s group, and funding from QUEST, PTB, LUH and NTH (project number 2.2.11).

-
- [1] W. Ketterle, D. S. Durfee and D. M. Stamper-Kurn, In *Proceedings of the 1998 Enrico Fermi summer school on Bose-Einstein condensation in Varenna, Italy*, pages 67–176. IOS Press, Amsterdam (1999).
 - [2] Pradip K. Ghosh: *Ion Traps*. International Series of Monographs on Physics. Clarendon Press, Oxford (1996).
 - [3] Sebastiaan Y. T. van de Meerakker *et al.*, Chemical Reviews **112**, 4828–4878 (2012).
 - [4] D. J. Berkeland *et al.*, Journal of Applied Physics **83**, 5025 (1998).
 - [5] József Fortágh and Claus Zimmermann, Reviews of Modern Physics **79**, 235 (2007).
 - [6] T. Calarco *et al.*, Physical Review A **61**, 022304 (2000).
 - [7] Philipp Treutlein *et al.*, Physical Review A **74**, 022312 (2006).
 - [8] Wilfried Maineult *et al.*, Physical Review Letters **109**, 020407 (2012).
 - [9] C. Ospelkaus *et al.*, Physical Review Letters **101**, 090502 (2008).
 - [10] C. Ospelkaus *et al.*, Nature **476**, 181–184 (2011).
 - [11] D. T. C. Allcock *et al.*, Applied Physics Letters **102**, 044103–044103-4 (2013).
 - [12] Pascal Böhi *et al.*, Applied Physics Letters **97**, 051101

- (2010).
- [13] U. Warring *et al.*, Physical Review A **87**, 013437 (2013).
 - [14] A. Walther *et al.*, Physical Review A **83**, 062329 (2011).
 - [15] D. I. Schuster *et al.*, Physical Review A **83**, 012311 (2011).
 - [16] D. Kielpinski *et al.*, Physical Review Letters **108**, 130504 (2012).
 - [17] M. Carsjens *et al.*, Applied Physics B **114**, 243–250 (2014).
 - [18] Philipp Treutlein, Ph.D. thesis, Ludwig-Maximilians-Universität München (2008).
 - [19] Hsiang-Yu Lo *et al.*, Applied Physics B **114**, 17–25 (2013).
 - [20] R. J. Hendricks *et al.*, Applied Physics B **88**, 507–513 (2007).
 - [21] C. Langer *et al.*, Physical Review Letters **95**, 060502 (2005).
 - [22] Florian Mintert and Christof Wunderlich, Physical Review Letters **87**, 257904 (2001).
 - [23] A. Khromova *et al.*, Physical Review Letters **108**, 220502 (2012).
 - [24] K. Lake *et al.*, Physical Review A **91**, 012319 (2015).
 - [25] J M Amini *et al.*, New Journal of Physics **12**, 033031 (2010).
 - [26] Nicholas D. Guise *et al.*, Journal of Applied Physics **117**, 174901 (2015).
 - [27] D. L. Moehring *et al.*, New Journal of Physics **13**, 075018 (2011).
 - [28] D. P. L. Aude Craik *et al.*, Applied Physics B **114**, 3–10 (2014).
 - [29] Manuel Mielenz *et al.*, arXiv:1512.03559 [physics, physics:quant-ph] (2015), arXiv: 1512.03559.
 - [30] R. Blatt and C. F. Roos, Nature Physics **8**, 277–284 (2012).
 - [31] Ch Schneider, Diego Porras and Tobias Schaetz, Reports on Progress in Physics **75**, 024401 (2012).
 - [32] David J. Wineland, Reviews of Modern Physics **85**, 1103–1114 (2013).
 - [33] C. Monroe and J. Kim, Science **339**, 1164–1169 (2013).